

A Navier-Stokes phase-field crystal model for colloidal suspensions

Simon Praetorius and Axel Voigt

Citation: *The Journal of Chemical Physics* **142**, 154904 (2015); doi: 10.1063/1.4918559

View online: <http://dx.doi.org/10.1063/1.4918559>

View Table of Contents: <http://scitation.aip.org/content/aip/journal/jcp/142/15?ver=pdfcov>

Published by the [AIP Publishing](#)

Articles you may be interested in

[Parabolized Navier–Stokes model for study the interaction between roughness structures and concentrated vortices](#)

Phys. Fluids **25**, 104103 (2013); 10.1063/1.4823746

[Short-time transport properties in dense suspensions: From neutral to charge-stabilized colloidal spheres](#)

J. Chem. Phys. **128**, 104903 (2008); 10.1063/1.2868773

[A smooth particle-mesh Ewald algorithm for Stokes suspension simulations: The sedimentation of fibers](#)

Phys. Fluids **17**, 033301 (2005); 10.1063/1.1862262

[Sedimentation equilibrium of a suspension of adhesive colloidal particles in a planar slit: A density functional approach](#)

J. Chem. Phys. **116**, 384 (2002); 10.1063/1.1421354

[Sedimentation potential of a concentrated spherical colloidal suspension](#)

J. Chem. Phys. **110**, 11643 (1999); 10.1063/1.479103



A Navier-Stokes phase-field crystal model for colloidal suspensions

Simon Praetorius^{a)} and Axel Voigt^{b)}

Institute of Scientific Computing, Technische Universität Dresden, D-01062 Dresden, Germany

(Received 26 January 2015; accepted 3 April 2015; published online 20 April 2015)

We develop a fully continuous model for colloidal suspensions with hydrodynamic interactions. The Navier-Stokes Phase-Field Crystal model combines ideas of dynamic density functional theory with particulate flow approaches and is derived in detail and related to other dynamic density functional theory approaches with hydrodynamic interactions. The derived system is numerically solved using adaptive finite elements and is used to analyze colloidal crystallization in flowing environments demonstrating a strong coupling in both directions between the crystal shape and the flow field. We further validate the model against other computational approaches for particulate flow systems for various colloidal sedimentation problems. © 2015 AIP Publishing LLC. [<http://dx.doi.org/10.1063/1.4918559>]

I. INTRODUCTION

Simple fluids can be coarse grained, considered as a continuum and very well described by the Navier-Stokes equations. A quantitative description can be achieved down to the nanometer scale. For colloidal suspensions, this simple treatment is not necessarily valid any more. Here, colloidal particles, with a typical size range of nanometers to a few microns, move due to collisions with the solvent molecules, interact with each other and induce flow fields due to their motion. It is shown that these hydrodynamic interactions are of relevance in various practical applications, e.g., colloidal gelation¹ or coagulation of colloidal dispersions.² To calculate nonequilibrium properties of such systems, it requires to resolve the different time and length scales arising from thermal Brownian motion and hydrodynamic interactions. Various approaches have been developed to consider these interactions in an effective way. For an overview and proposed coarse-graining descriptions, see e.g., Ref. 3.

One of the most popular approaches is Stokesian dynamics (SD) within the low Reynolds number limit.⁴ The hydrodynamic interaction is thereby incorporated in an approximate analytical form, assuming to result as the sum of two-body interactions. The approach is difficult to implement for complex boundary conditions and is relatively expensive. As an alternative, direct numerical simulations are proposed, which involve determining fluid motion simultaneously with particle motion. In these methods, the colloidal particles are fully resolved and coupled with the Navier-Stokes equations, leading to coupled discrete-continuous descriptions. Other discrete and hybrid models are, e.g., the (smoothed) dissipative particle dynamics model,^{5–7} the fictitious domain/immersed boundary method,^{8,9} and the Lattice Boltzmann-molecular dynamics method.^{10–12} A short review and comparison of such models is given in Ref. 13.

Our aim is to derive a fully continuous system of equations from such hybrid models. This has the advantage of an efficient

numerical treatment, the possibility of a detailed numerical analysis, and it offers a straight forward coupling with other fields. The model will serve as a general continuum model for colloidal suspension, providing a quantitative approach down to the length scale set by the colloidal particles and it is operating on diffusive time scales. The approach will be derived by combining ideas from: (a) dynamic density functional theory (DDFT) and (b) hybrid discrete-continuous particulate flow models. We will test the derived system for colloidal crystallization in flowing environments and for colloidal sedimentation.

A. Dynamic density functional theory approach

The aim of the DDFT approach is to provide a reduced model that describes the local state of a colloidal fluid by the time averaged one-particle density. The evolution of this density is driven by a gradient-flow of the equilibrium Helmholtz free-energy functional. A first realization of a DDFT for colloidal fluids is presented in the work of Marconi and Tarazona¹⁴ with colloids modeled as Brownian particles. Later, this theory has been extended by Archer¹⁵ and has been connected to the equations of motion from continuum fluid mechanics. Rauscher¹⁶ described an advected DDFT, to model colloids in a flowing environment, that do not interact via hydrodynamic interactions. The work of Goddard *et al.*¹⁷ incorporates the effect of inertia and hydrodynamic interactions between the colloidal particles, and recently Gránásy *et al.*¹⁸ have explored a coarse-grained density coupling of DDFT and the Navier-Stokes equations.

We start the derivation of our model with the dynamical equations derived by Archer.¹⁵ Therefore, we introduce the one-particle (number) density $\varrho(\mathbf{r}, t)$ and the average local velocity $\mathbf{v}(\mathbf{r}, t)$ of the colloidal particles. The density is driven by a continuity equation

$$\partial_t \varrho + \nabla \cdot (\varrho \mathbf{v}) = 0, \quad (1)$$

with the current, expressed as $\varrho \mathbf{v}$, evolving by the dynamical equation

^{a)}simon.praetorius@tu-dresden.de

^{b)}axel.voigt@tu-dresden.de

$$m\varrho(\partial_t \mathbf{v} + (\mathbf{v} \cdot \nabla)\mathbf{v} + \gamma \mathbf{v}) = -\varrho \nabla \frac{\delta \mathcal{F}_H[\varrho]}{\delta \varrho} + \eta \Delta \mathbf{v}, \quad (2)$$

where m represents the mass of the particles, γ a dumping coefficient, $\mathcal{F}_H[\varrho]$ the equilibrium Helmholtz free-energy functional, and η a viscosity coefficient.

We use a minimal expression for the free-energy, the Swift-Hohenberg (SH) energy,^{19,20} in a dimensionless form

$$\mathcal{F}_H[\varrho(\psi)] \simeq \mathcal{F}_{sh}[\psi] = \int \frac{1}{4}\psi^4 + \frac{1}{2}\psi(r + (q_0^2 + \Delta)^2)\psi \, d\hat{\mathbf{r}}, \quad (3)$$

with $\varrho = \bar{\varrho}(1 + (\psi + 0.5))$, a parametrization of the one-particle density with respect to a reference density $\bar{\varrho}$. The phenomenological parameter r is related to the undercooling of the system and the constant q_0 is related to the lattice spacing. This functional arises by splitting the energy in an ideal gas contribution and an excess free energy $\mathcal{F}_H = \mathcal{F}_{id} + \mathcal{F}_{exc}$, rescaling and shifting of the order-parameter ϱ , expanding ideal gas contributions in real-space, and the excess free energy in Fourier-space and simplification by removing constant and linear terms that would vanish in the dynamical equations. A detailed derivation of the energy can be found in Refs. 21–23.

Inserting the density expansion and free-energy (3) into (1) and (2), we get a system of dynamic equations for the density deviation ψ and the related non-dimensionalized averaged velocity $\hat{\mathbf{v}}$,

$$\partial_t \psi + \nabla \cdot ((1.5 + \psi)\hat{\mathbf{v}}) = 0, \quad (4)$$

$$(1.5 + \psi)(\partial_t \hat{\mathbf{v}} + (\hat{\mathbf{v}} \cdot \nabla)\hat{\mathbf{v}} + \Gamma \hat{\mathbf{v}}) = \frac{1}{Re} \Delta \hat{\mathbf{v}} - \frac{1}{Pe} (1.5 + \psi) \nabla \frac{\delta \mathcal{F}_{sh}[\psi]}{\delta \psi}. \quad (5)$$

With respect to a length scale L and time scale L/V_0 , we have the dimensionless variable $\hat{\mathbf{v}} = \mathbf{v}/V_0$, and Peclet number Pe , Reynolds number Re , and friction coefficient Γ given by

$$Pe = \frac{3mV_0^2}{k_B T}, \quad Re = \frac{m\bar{\varrho}LV_0}{\eta}, \quad \Gamma = \frac{\gamma L}{V_0},$$

with Boltzmann's constant k_B and temperature T . In Appendix A, a detailed derivation of this dimensionless form of the dynamical equations can be found.

In the overdamped limit, $\Gamma \gg 1$, the velocity equation reduces to an explicit expression that relates the velocity to the chemical potential by

$$(1.5 + \psi)\hat{\mathbf{v}} = -\frac{1}{\Gamma Pe} (1.5 + \psi) \nabla \frac{\delta \mathcal{F}_{sh}[\psi]}{\delta \psi}. \quad (6)$$

Inserting (6) into (4) results in the Phase-Field Crystal (PFC) equation²⁰

$$\partial_t \psi = \frac{1}{\Gamma Pe} \nabla \cdot \left((1.5 + \psi) \nabla \frac{\delta \mathcal{F}_{sh}[\psi]}{\delta \psi} \right), \quad (7)$$

referred to as PFC1 model in Ref. 21.

B. Particulate flows

Typical approaches to simulate particulate flows on larger length scales consider a Newton-Euler equation for each particle to describe their motion as a rigid body and combine

this with a Navier-Stokes solver for the flow around these particles. Various numerical approaches have been proposed to model this flow and the incorporation of a no-slip boundary condition on the particle surfaces, see, e.g., Refs. 24–27. Examples for numerical approaches are the fictitious domain and the immersed boundary method. All these approaches use the general idea to consider the particles as a highly viscous fluid, which allows the flow computation to be done on a fixed space region. The no-slip boundary condition on the particle surface is thereby enforced directly or implicitly, depending on the numerical approach. All these methods combine a continuous description of the flow field with a discrete off-lattice simulation for the particles.

Considering an incompressible fluid with viscosity η_f and constant fluid density ρ_f , we can write the Navier-Stokes equations for velocity \mathbf{u} and pressure p of a pure fluid in a dimensionless form,

$$\partial_t \hat{\mathbf{u}} + (\hat{\mathbf{u}} \cdot \nabla)\hat{\mathbf{u}} = -\nabla \hat{p} + \frac{1}{Re_f} \nabla \cdot (2(1 + \tilde{\eta})\mathbf{D}(\hat{\mathbf{u}})) + \mathbf{F}, \quad (8)$$

$$\nabla \cdot \hat{\mathbf{u}} = 0, \quad (9)$$

with length and time scale as above and the dimensionless velocity field $\hat{\mathbf{u}} = \mathbf{u}/V_0$, the viscosity perturbation $\tilde{\eta}$ from the expansion $\eta_f = \bar{\eta}_f(1 + \tilde{\eta})$, and the fluid Reynolds number Re_f and the dimensionless pressure \hat{p} given by

$$Re_f = \frac{\rho_f LV_0}{\bar{\eta}_f}, \quad \hat{p} = \frac{p}{\rho_f V_0^2},$$

respectively. The expression $\mathbf{D}(\hat{\mathbf{u}})$ gives the symmetric part of the velocity gradient, i.e.,

$$\mathbf{D}(\hat{\mathbf{u}}) = \frac{1}{2}(\nabla \hat{\mathbf{u}} + \nabla \hat{\mathbf{u}}^\top)$$

and \mathbf{F} defines a volume force.

As a reference model for colloidal suspensions, we consider the fluid particle dynamics (FPD) model by Ref. 28. Here, the particles are considered as a highly viscous fluid and the velocities of the particles are extracted from the fluid velocity \mathbf{u} . The shape of the particles is constructed using a tanh-profile with a specified radius and interface thickness and their centers of mass interact via an interparticle potential. The approach can also be seen as a modification of a classical “model H,”^{29,30} with a fluid and a particle phase and the driving force in the Navier-Stokes equations governed by the interatomic potential. The approach again combines continuous and discrete descriptions.

The motion of colloidal particles with positions $\mathbf{r}_i(t)$ are governed by the velocities $\mathbf{v}_i(t)$ and the evolution of a flow field \mathbf{u} , where the colloidal particles are suspended in. The basic idea is to introduce concentration fields $\phi_i(\mathbf{r}, t) \in [0, 1]$ for each particle and to average the fluid velocity over regions with high concentration, i.e.,

$$\mathbf{v}_i(t) = \frac{\int \phi_i(\mathbf{r}, t) \mathbf{u}(\mathbf{r}, t) \, d\mathbf{r}}{\int \phi_i(\mathbf{r}, t) \, d\mathbf{r}}.$$

Thus, the motion of the particles can be described by $\mathbf{r}_i(t + \Delta t) := \mathbf{r}_i(t) + \Delta t \cdot \mathbf{v}_i(t)$, with Δt the simulation time step.

A space-dependent fluid viscosity η_f , as a function of ϕ_i , is introduced to describe the rigidity of the particles, and a

force term $\mathbf{F} := \mathbf{F}^{[\text{ta}]}$ to account for the particle interactions in flow equation (8). This force is chosen as the negative gradient of an interaction potential \mathcal{V} , multiplied with the particle-concentration fields ϕ_i ,

$$\mathbf{F}^{[\text{ta}]}(\mathbf{r}) \stackrel{\text{def}}{=} - \sum_i \nabla_{\mathbf{r}_i} \left(\sum_{j \neq i} \mathcal{V}(\|\mathbf{r}_i - \mathbf{r}_j\|) \right) \phi_i(\mathbf{r}). \quad (10)$$

The fluid viscosity $\eta_f = \bar{\eta}_f(1 + \bar{\eta})$ is modeled, by describing the viscosity perturbation $\bar{\eta}$, as

$$\bar{\eta}(\mathbf{r}) = \sum_i \left(\frac{\bar{\eta}_p}{\bar{\eta}_f} - 1 \right) \phi_i(\mathbf{r}), \quad (11)$$

with $\bar{\eta}_f < \bar{\eta}_p$ the liquid and particle viscosity, respectively. In Ref. 31, it is argued that the artificial diffusivity $\bar{\eta}_p/\bar{\eta}_f$ must go to ∞ for the particles to become rigid. In their method, they have introduced a different body force to guarantee this rigidity without taking large values of the viscosity ratio. However, we will here only consider the original FPD approach.

C. Towards a fully continuous description

Our aim is to derive a fully continuous model by combining the FPD model with the PFC approach. A first step in this direction has already been done in Ref. 32, where the interaction potential has already been replaced by the PFC approach. The discrete off-lattice simulation for the particles is no longer needed; the particle positions and velocities result from the advected PFC model. However, the forcing term in the Navier-Stokes equations still requires the identification of the position and velocity of each particle, and thus the approach still has a discrete component. To derive a fully continuous model, we will first clarify the relation of the different approaches in Refs. 23, 28, and 32 and will show that all the discrete coupling terms can be approximated with a simple continuous expression.

To allow for a description of the flow of individual particles, we consider a variant of the PFC model, the vacancy PFC model, introduced in Refs. 33 and 34. Instead of minimizing the Swift-Hohenberg functional directly, we consider a density field with positive density deviation ψ , only, which leads to a modification of the particle-interaction and allows to handle single particles, as well as many individual particles embedded in the fluid.

II. DERIVATION OF A FULLY CONTINUOUS MODEL

In Ref. 32, the PFC model and the FPD model are combined, by letting the density field influence the flow field. The interatomic potential is encoded in Swift-Hohenberg energy (3) and the particle positions evolve according to the advective PFC equation (see below). The forcing term $\mathbf{F} := \mathbf{F}^{[\text{ml}]}$ in the Navier-Stokes equations now ensures the fluid velocity \mathbf{u} to be equal to the particle velocity \mathbf{v}_i at the particle position \mathbf{r}_i , i.e.,

$$\mathbf{F}^{[\text{ml}]}(\mathbf{r}) \stackrel{\text{def}}{=} \omega \sum_i (\hat{\mathbf{v}}_i - \hat{\mathbf{u}}(\mathbf{r})) \delta(\mathbf{r} - \mathbf{r}_i), \quad (12)$$

with $\omega \gg 1$ a penalty parameter and $\delta(\cdot)$ the pointwise delta-function. Thereby, position and velocity of each individual particle must be extracted from the density field ψ by tracking the

maxima of the density that are interpreted as average particle positions. These quantities are then explicitly inserted into the expression of the forcing term. The fluid viscosity η_f can be modeled as before in (11), but now ψ can directly be used to distinguish between the background fluid and the particles.

Force term (12) constrains the fluid velocity to be equal to the particle velocity at the center-of-mass position of the particle. In order to implement a no-slip boundary condition at the particle surfaces, the delta function needs to be replaced by the concentration fields $\phi_i(\mathbf{r})$,

$$\mathbf{F}^{[\text{ddl}]}(\mathbf{r}) \stackrel{\text{def}}{=} \omega \sum_i (\hat{\mathbf{v}}_i - \hat{\mathbf{u}}(\mathbf{r})) \phi_i(\mathbf{r}). \quad (13)$$

This ansatz is highly related to the diffuse domain approach,³⁵ where this force is shown to converge to the no-slip boundary condition $\mathbf{u} = \mathbf{v}_i$ at the i -th particle surface, if the interface width goes to zero. Thereby, ω has to be related to the interface thickness, see Ref. 36 for a detailed convergence study.

In the following, we give a new formulation of a continuous force term that can be evaluated without extracting individual particle positions and velocities. At first, we relate the density field ψ , described in (7), to a delta function $\delta(\mathbf{r})$ and to a concentration field $\phi(\mathbf{r}) = \sum_i \phi_i(\mathbf{r})$. In a second step, the particle velocities are shown to arise directly from the evolution equations (7) and (6), respectively.

A. Approximation of a delta-function

For the classical PFC equation in 1D, a one-mode approximation of the density ψ is given by Ref. 37

$$\psi_{\text{om}}(\mathbf{r}) = A \cos(q_0 \mathbf{r}) + \bar{\psi}, \quad (14)$$

where A, q_0 , and $\bar{\psi}$ are constants that define the amplitude, lattice constant, and mean density of the field, respectively. We introduce

$$\psi_{(0)} = \frac{1}{2} \left(1 + \frac{\psi_{\text{om}} - \bar{\psi}}{A} \right), \quad \psi_{(k)} = (\psi_{(k-1)})^2, \quad (15)$$

for $k > 0$, or in explicit form $\psi_{(k)} = [\psi_{(0)}]^{2^k}$ for $k \in \mathbb{N}$. After appropriate normalization, we obtain

$$\delta_{(k)}(\mathbf{r}) := N_k \psi_{(k)}(\mathbf{r}), \quad (16)$$

with N_k normalization constants that ensure the property $\int \delta_{(k)}(\mathbf{r}) d\mathbf{r} = 1$. Values for various indices k can be found in Table I. Thus, we have a sequence of nascent delta functions. Figure 1 shows the first three elements of this sequence in comparison with the classical Gaussians $\delta_\epsilon^{\text{xp}}(\mathbf{r}) \cong e^{[(q_0 \|\mathbf{r}\|)^2 / (-4\epsilon)]}$, visualizing the convergence qualitatively. As a consequence of this property, the shifted and scaled density field $\psi_{(0)}$ can be seen as a first-order approximation of a delta function. The approach can be generalized to 2D and 3D and will be used for ψ instead of ψ_{om} .

TABLE I. The first four elements of the sequence N_k , the normalization constants for the nascent delta function $\delta_{(k)}$.

k	0	1	2	3
$N_k \cdot \frac{\pi}{q_0}$	1	$\frac{4}{3}$	$\frac{64}{35}$	$\frac{16384}{6435}$

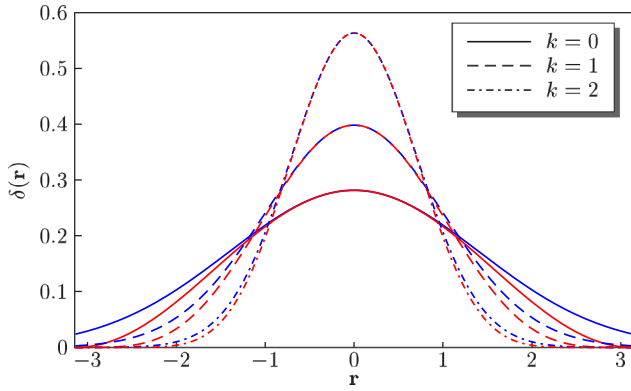


FIG. 1. The first three elements of the sequences $\delta_{\epsilon_k}^{\text{exp}}$ (normalized), with $\epsilon_k = 2^{-k}$, in blue (upper curves) and $\delta_{(k)}$ in red (lower curves). The lattice constant is $q_0 = 1$.

B. Approximation of concentration fields

The concentration field ϕ_i in Ref. 28, used for the phase-field description of particles, is defined by

$$\phi_i(\mathbf{r}) = \frac{1}{2} \left(1 - \tanh\left(\frac{\|\mathbf{r} - \mathbf{r}_i\| - a}{\epsilon}\right) \right), \quad (17)$$

with \mathbf{r}_i the center-of-mass position of the i -th particle, a the particle radius and ϵ a small parameter that defines the width of the smoothing region. We now interpret $\psi_{(0)}$ in (15) as a concentration field. It has the value one at the maxima of the cosine profile and zero in between. The transition is very coarse but gives an approximation of the tanh-profile of $\phi(\mathbf{r}) = \sum_i \phi_i(\mathbf{r})$, which can be refined with

$$\phi(\psi) = \frac{1}{2} \left(1 + \tanh\left(\frac{(\psi_{(0)} - \sigma)}{\epsilon}\right) \right), \quad (18)$$

where $\sigma = \frac{1}{2}(1 + \cos(q_0 \cdot a))$ is a shifting parameter, see Figure 2 for an example of such an implementation.

In order to define the viscosity field, we adopt expression (11) and insert for $\phi(\mathbf{r})$ the field $\phi(\psi)$. Thus, we introduce a viscosity field depending directly on the PFC density field ψ , using transformation (18) as

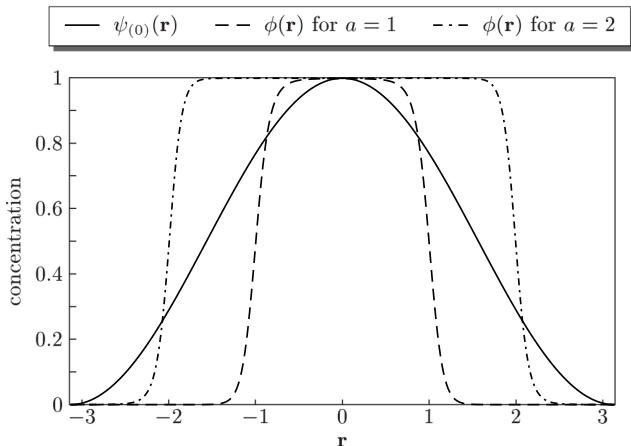


FIG. 2. Transformation of the density field ψ into a tanh-concentration field, for different particle radii. The lattice constant is $q_0 = 1$ and interface width $\epsilon = 0.1$.

$$\tilde{\eta}(\mathbf{r}) = \tilde{\eta}(\psi(\mathbf{r})) = \left(\frac{\tilde{\eta}_p}{\tilde{\eta}_f} - 1 \right) \phi(\psi). \quad (19)$$

C. Peak velocities

To approximate the particle velocities \mathbf{v}_i , we follow the approach of Rauscher³⁸ and consider a curl-free velocity field for the derivation. Let \mathbf{u} be given with the property $\nabla \times \mathbf{u} = 0$ and $\nabla \cdot \mathbf{u} = 0$. Then, there exists a potential field Ψ such that

$$\mathbf{u} = -\frac{1}{\gamma m} \nabla \Psi, \quad \Delta \Psi = 0. \quad (20)$$

Following the argumentation of Ref. 38, the flow potential Ψ acts as an external potential that drives the particle density. In DDFT models, this external potential enters the free-energy by $\mathcal{F}^*[\varrho] := \mathcal{F}_H[\varrho] + \mathcal{F}_{\text{ext}}[\varrho]$, with

$$\mathcal{F}_{\text{ext}}[\varrho] = \int \Psi(\mathbf{r}) \varrho \, d\mathbf{r}.$$

Inserting \mathcal{F}^* into (2) instead of \mathcal{F}_H leads to

$$\begin{aligned} m\varrho(\partial_t \mathbf{v} + (\mathbf{v} \cdot \nabla) \mathbf{v} + \gamma \mathbf{v}) &= -\varrho \nabla \frac{\delta \mathcal{F}^*[\varrho]}{\delta \varrho} + \eta \Delta \mathbf{v} \\ &= -\varrho \nabla \frac{\delta \mathcal{F}_H[\varrho]}{\delta \varrho} - \varrho \nabla \Psi + \eta \Delta \mathbf{v} \\ &= -\varrho \nabla \frac{\delta \mathcal{F}_H[\varrho]}{\delta \varrho} + \gamma m \varrho \mathbf{u} + \eta \Delta \mathbf{v} \end{aligned}$$

and finally we arrive at

$$m\varrho(\partial_t \mathbf{v} + (\mathbf{v} \cdot \nabla) \mathbf{v} + \gamma(\mathbf{v} - \mathbf{u})) = -\varrho \nabla \frac{\delta \mathcal{F}_H[\varrho]}{\delta \varrho} + \eta \Delta \mathbf{v}.$$

Going to the dimensionless form, by introducing length and time scales and inserting \mathcal{F}_{sh} for \mathcal{F}_H gives

$$\partial_t \psi + \nabla \cdot ((1.5 + \psi) \hat{\mathbf{v}}) = 0, \quad (21)$$

$$\begin{aligned} (1.5 + \psi)(\partial_t \hat{\mathbf{v}} + (\hat{\mathbf{v}} \cdot \nabla) \hat{\mathbf{v}} + \Gamma(\hat{\mathbf{v}} - \hat{\mathbf{u}})) &= \frac{1}{Re} \Delta \hat{\mathbf{v}} \\ - \frac{1}{Pe} (1.5 + \psi) \nabla \frac{\delta \mathcal{F}_{\text{sh}}[\psi]}{\delta \psi} &. \end{aligned} \quad (22)$$

In the overdamped limit, $\Gamma \gg 1$, velocity equation (22) reduces to a simple expression for the velocity $\hat{\mathbf{v}}$,

$$\Gamma(\hat{\mathbf{v}} - \hat{\mathbf{u}}) \simeq -\frac{1}{Pe} \nabla \frac{\delta \mathcal{F}_{\text{sh}}[\psi]}{\delta \psi}. \quad (23)$$

Inserting this into (21) results in the advected PFC equation introduced in Ref. 23 and considered in the context of DDFT in Ref. 16,

$$\begin{aligned} \partial_t \psi + \hat{\mathbf{u}} \cdot \nabla \psi &= \frac{1}{\Gamma Pe} \nabla \cdot \left((1.5 + \psi) \nabla \frac{\delta \mathcal{F}_{\text{sh}}[\psi]}{\delta \psi} \right) \\ &= \nabla \cdot \left(M(\psi) \nabla \frac{\delta \mathcal{F}_{\text{sh}}[\psi]}{\delta \psi} \right), \end{aligned} \quad (24)$$

with a mobility function $M(\psi) = \frac{1}{\Gamma Pe} (1.5 + \psi)$.

Although this equation can only be derived for potential flows, we will use it as an approximate model for non-potential flows as well. With (23), we have found an explicit expression for the mean velocity of the particles that can be used to formulate forcing term (12) in the continuous form

$$\begin{aligned}
\mathbf{F}^{[\text{ml}]}(\mathbf{r}) &= \omega \sum_i (\hat{\mathbf{v}}_i - \hat{\mathbf{u}}(\mathbf{r})) \delta(\mathbf{r} - \mathbf{r}_i) \\
&\approx -\frac{\omega}{\Gamma Pe} \nabla \frac{\delta \mathcal{F}_{\text{sh}}[\psi]}{\delta \psi} \sum_i \delta(\mathbf{r} - \mathbf{r}_i) \\
&\approx -\frac{\omega}{\Gamma Pe} \nabla \frac{\delta \mathcal{F}_{\text{sh}}[\psi]}{\delta \psi} \delta_{(k)}, \quad (25)
\end{aligned}$$

with $\delta_{(k)}$ nascent delta function (16) approximating $\delta_\Omega = \sum_i \delta(\mathbf{r} - \mathbf{r}_i)$. The first-order approximation of this force, with

$$\delta_{(0)} \approx N_0 \psi_{(0)} = \frac{q_0}{\pi} \psi_{(0)} = \frac{q_0}{2\pi} \left(1 + \frac{1}{A}(\psi - \bar{\psi})\right),$$

thus reads

$$\mathbf{F}_{(0)}^{[\text{ml}]}(\mathbf{r}) = -(M_0 + M_1 \psi) \nabla \psi^{\text{h}}(\mathbf{r}), \quad (26)$$

with $M_0 = (1 - \bar{\psi}/A) \frac{\omega}{\Gamma Pe} \frac{q_0}{2\pi}$, $M_1 = \frac{\omega}{\Gamma Pe} \frac{q_0}{2\pi A}$, and $\psi^{\text{h}} := \frac{\delta \mathcal{F}_{\text{sh}}[\psi]}{\delta \psi}$, which results in the considered fully continuous description. For $\omega \sim \Gamma$, we have $M_1 = \mathcal{O}(\frac{1}{Pe})$.

D. Individual particles and number of particles

In order to allow for particles to move freely, we add a modification introduced by Ref. 33. The authors have argued that by limiting the field ψ from below, the particle interaction can be modified. Therefore, they have introduced the constraint $\psi \geq 0$, which allows to control the volume fraction of particles in the domain by changing the mean density of the system.

To implement the constraint, the free-energy is modified by including a penalty term, i.e., $\mathcal{F}_{\text{vpfc}} := \mathcal{F}_{\text{sh}} + \mathcal{F}_{\text{penalty}}$, with

$$\mathcal{F}_{\text{penalty}}[\psi] = \int \beta (|\psi|^n - \psi^n) \, d\mathbf{r},$$

with $\beta \gg 1$ and n an odd integer exponent.

The variational derivative of $\mathcal{F}_{\text{penalty}}$ can be found to be

$$b(\psi) := \frac{\delta \mathcal{F}_{\text{penalty}}[\psi]}{\delta \psi} = n\beta \psi^{n-1} (\text{sign}(\psi) - 1), \quad (27)$$

$$\text{with } \text{sign}(\psi) = \begin{cases} 1, & \text{for } \psi > 0, \\ 0, & \text{for } \psi = 0, \\ -1, & \text{for } \psi < 0. \end{cases}$$

While localized states are also observed in the original PFC model for a small range of parameters in the coexistence regime,³⁹ we consider the approach in Refs. 33, 34, and 40 using penalty term (27). Here, the number of particles can be controlled by choosing the mean density and the area the particles occupy. The initial density field for a collection of N particles located at the positions \mathbf{r}_i , $i = 1, \dots, N$, is a composition of local density peaks,

$$\psi_0^{(i)}(\mathbf{r}) = \begin{cases} A \cdot \left(\cos\left(\frac{\sqrt{3}q_0}{2} \|\mathbf{r} - \mathbf{r}_i\|\right) + 1\right) & \text{for } \|\mathbf{r} - \mathbf{r}_i\| < \frac{d}{2} \\ 0 & \text{otherwise,} \end{cases}$$

summed up to $\psi(\mathbf{r}) = \sum_{i=1}^N \psi_0^{(i)}(\mathbf{r})$.

Thus, each particle occupies an area of approximately $B_p := \pi(d/2)^2$ in 2D. Based on the ideas in Ref. 33, we set the mean density in the particle domain to $\psi_1 = \sqrt{(-48 - 56r)/133}$, as well as $r = -0.9$ and $q_0 = 1$. The last two parameters define the mean density of the system as

$$\bar{\psi} = \frac{N \cdot B_p}{B_0} \psi_1,$$

with $B_0 = |\Omega|$ the area of the computational domain Ω and with $A = \psi_1$ the parameter for the density scaling.

E. Navier-Stokes PFC model

Combining all the components, i.e., the Navier-Stokes equation for solvent (8) with viscosity η given by $\eta(\psi)$ in (19), and volume force \mathbf{F} by expression (26), combined with density evolution (24) with \mathcal{F}_{sh} or $\mathcal{F}_{\text{vpfc}}$, results in the fully continuous Navier-Stokes PFC (NS-PFC) model

$$\begin{aligned}
\partial_t \hat{\mathbf{u}} + (\hat{\mathbf{u}} \cdot \nabla) \hat{\mathbf{u}} &= \nabla \cdot \hat{\boldsymbol{\sigma}} - M_1 \psi \nabla \psi^{\text{h}}, \\
\nabla \cdot \hat{\mathbf{u}} &= 0, \\
\partial_t \psi + \hat{\mathbf{u}} \cdot \nabla \psi &= \nabla \cdot (M(\psi) \nabla \psi^{\text{h}}), \\
\psi^{\text{h}} &= \frac{\delta \mathcal{F}_{\text{sh/vpfc}}[\psi]}{\delta \psi}, \quad (28)
\end{aligned}$$

with

$$\begin{aligned}
\hat{\boldsymbol{\sigma}} &= -\tilde{p} \mathbf{I} + \frac{1}{Re_f} (1 + \tilde{\eta}(\psi)) (\nabla \hat{\mathbf{u}} + \nabla \hat{\mathbf{u}}^{\text{T}}), \\
\frac{\delta \mathcal{F}_{\text{sh}}[\psi]}{\delta \psi} &= \psi^3 + (r + (1 + \Delta)^2) \psi, \\
\frac{\delta \mathcal{F}_{\text{vpfc}}[\psi]}{\delta \psi} &= \psi^3 + (r + (1 + \Delta)^2) \psi + b(\psi),
\end{aligned}$$

and $\tilde{p} = \hat{p} + M_0 \psi^{\text{h}}$ a rescaled pressure. Besides the definition of ψ^{h} , these equations have exactly the form of ‘‘model H’’ as considered in Ref. 41. In Appendix B, we demonstrate thermodynamic consistency of the derived model.

III. NUMERICAL STUDIES

We now turn to quantitative properties of the model and compare it with the original PFC model and the FPD approach of Ref. 28 for various situations. We rewrite the NS-PFC system as a system of second order equations. Therefore, the variational derivatives are implemented as

$$\begin{aligned}
\frac{\delta \mathcal{F}_{\text{sh}}[\psi]}{\delta \psi} &= \psi^3 + (r + 1) \psi + 2\Delta \psi + \Delta v, \\
\frac{\delta \mathcal{F}_{\text{vpfc}}[\psi]}{\delta \psi} &= \psi^3 + (r + 1) \psi + 2\Delta \psi + \Delta v + b(\psi), \\
v &= \Delta \psi.
\end{aligned}$$

System (28) has to be solved for \mathbf{u} , \tilde{p} , ψ , ψ^{h} , and v in a domain Ω with boundary conditions depending on the specific example. To numerically solve this system of partial differential equations, we apply here an operator splitting approach⁴² with a sequential splitting, where we solve the PFC equations first, followed by the Navier-Stokes equations. In time, we use a semi-implicit backward Euler discretization with a linearization of all nonlinear terms, i.e., a one-step Newton iteration. In space, we discretize using a finite element method, with Lagrange elements, e.g., a P^2/P^1 Taylor-Hood element for the Navier-Stokes equation and a P^2 element for ψ , ψ^{h} , and v in the PFC equation. We further use adaptive mesh refinement, leading to an enhanced resolution along the particles. The system is solved using the parallel adaptive finite element framework AMDiS.^{43,44}

A. Crystallization

The first numerical examples use \mathcal{F}_{sh} and consider crystallization processes in flowing environments. The fluid is driven by boundary conditions. In the first case, we consider a rotating fluid, i.e., a gyre flow and in the second case, a Poiseuille flow with a parabolic inflow velocity profile.

1. Rotating crystals

A crystal grain is placed in a rotating fluid initially given by

$$\partial_t \mathbf{r} = \mathbf{u}_0(x, y) = \begin{pmatrix} C \sin(\pi \frac{x}{\text{dim}_x}) \cos(\pi \frac{y}{\text{dim}_y}) \\ -C \cos(\pi \frac{x}{\text{dim}_x}) \sin(\pi \frac{y}{\text{dim}_y}) \end{pmatrix} \quad (29)$$

in a domain $(x, y) \in \Omega = [0, \text{dim}_x] \times [0, \text{dim}_y]$. For the numerical experiment, we have chosen $\text{dim}_x = \text{dim}_y = 42d$. The boundary conditions for the Navier-Stokes equations are set by \mathbf{u}_0 .

We start the growth process with an initial grain of radius $2d$ in an undercooled environment with parameters $r = -0.3$ and mean density $\bar{\psi} = -0.35$. The mobility function is set to $M(\psi) = \psi + 1.5$ and the force scaling to $M_1 = 1$. The fluid Reynolds number is set to $Re_f = 1$ and the viscosity ratio to $\bar{\eta}_p/\bar{\eta}_f = 100$. For the concentration field that defines the profile of the viscosity, we have used an approximation of $\psi_{(0)}$,

$$\phi := \psi_{(0)} \approx \frac{\psi - \min_{\Omega}(\psi)}{\max_{\Omega}(\psi) - \min_{\Omega}(\psi)}.$$

Thus, the fluid viscosity is high in particles, low in between particles, and takes an intermediate value in the isotropic phase away from the crystal. However, other definitions of the viscosity parameter are possible as well.

In Fig. 3, the growth shapes for different velocities C are shown at the same simulation time. For a still fluid ($C = 0$), i.e., no advection, the final shape is the largest and the size of the crystal decreases for increasing velocity. For the largest considered velocity $C = 1$, the faceting of the crystal is also more pronounced than for the case of no induced fluid flow. The stationary images also show that the crystal rotates during the growth process. This can be seen at the varying crystal orientations in (a), (b), and (c) indicated by the white angle.

The growth process is analyzed in Fig. 4, showing the radius of the growing crystal over simulation time. The growth velocity strongly depends on the induced fluid velocity, as shown in the inlet plot of Fig. 4. The crystal grows slower for a

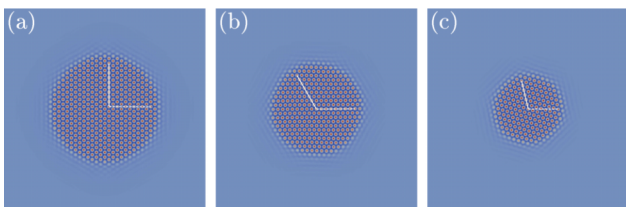


FIG. 3. Final growth-shapes of the crystal in a flowing environment at time $t = 3000$. Shown is the particle density ψ with color red corresponds to high density and blue to low density. The fluid velocity denoted by C : (a) $C = 0$, (b) $C = 0.5$, and (c) $C = 1$. The white angles show the crystal orientation and thus give an indication for crystal rotation.

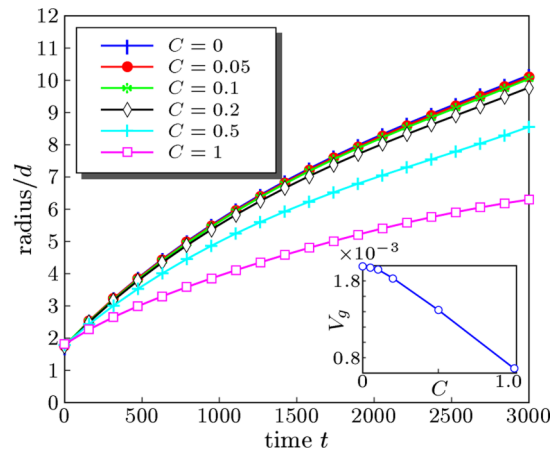


FIG. 4. Radius of the crystal divided by lattice constant over dimensionless time, for various fluid velocities C . In the inset, the growth velocity of the crystal normalized by the lattice constant V_g is shown for the final time $t = 3000$.

larger induced fluid velocity. This clearly shows one direction of the coupling, i.e., the fluid influences the crystallization.

The opposite can be found as well. The crystal also changes the velocity profile of the fluid. In the inlet of Fig. 5, the velocity profiles of two fluids are compared. The left image shows the profile of a fluid with no backcoupling of the density field to the Navier-Stokes equations. This essentially shows the initial profile \mathbf{u}_0 . The right image shows the velocity profile for the full NS-PFC model with $C = 1$. We observe different magnitudes of the velocity, whereas the streamlines do not change qualitatively. A more detailed analysis of the velocity profile along the x -axis from the center to the boundary of the domain can be found in Fig. 5. With fluid coupling, a linear increase of the magnitude in the domain of the crystal is observed, indicated by the black dashed line, which is

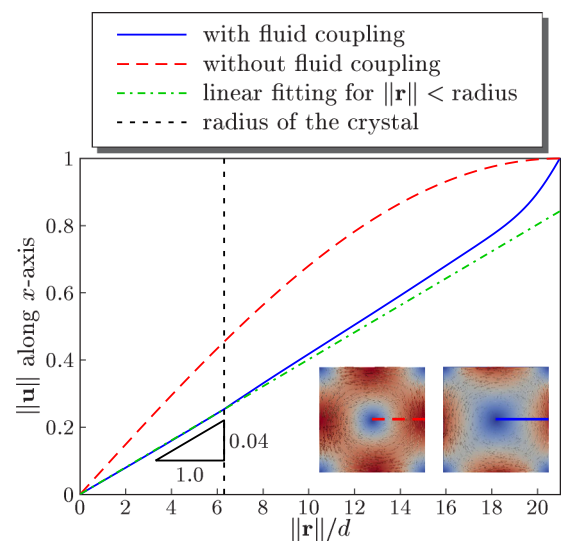


FIG. 5. Fluid velocity at time $t = 3000$ extracted from positive x -axis, as indicated by the lines in the inlet pictures. The slope 0.04 corresponds to the angular velocity of the fluid in the region with a radius less than the crystal radius. In the inlet, the magnitude of fluid velocity in the domain Ω for $C = 1$ is shown. Left: fluid flow not influenced by the crystal. Right: crystal slows down the fluid due to higher viscosity in the region of particles.

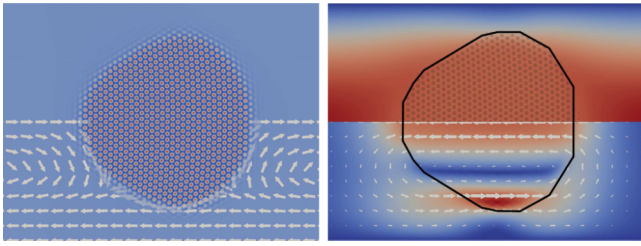


FIG. 6. Crystal shape and corresponding velocity profile at time $t = 3800$ in a narrow channel. Left: density field ψ , with arrows in the lower half corresponding to $\mathbf{u} - \mathbf{v}_{\text{crystal}}$, i.e., fluid velocity relative to the translation velocity of the crystal. Right: fluid velocity \mathbf{u} with contour line that indicates the shape of the crystal. In the lower half, the velocity relative to the channel flow velocity, i.e., $\mathbf{u} - \mathbf{u}_0$, is shown. Color red corresponds to high values and blue to low values.

lower than the prescribed initial profile. The crystal acts as a rotating solid in the fluid, with normalized angular velocity $\omega = \|\mathbf{u}\|/(\|\mathbf{r}\|/d) = 0.04$. Away from the crystal, the velocity increases up to the prescribed boundary velocity C .

2. Translating crystals

In the second case, the crystal grows in a Poiseuille flow. In a narrow channel, we enforce a parabolic velocity at the inflow boundary, i.e.,

$$\mathbf{u}_0(x, y) = (4C\bar{y}(1 - \bar{y}), 0)^T, \quad \bar{y} := \frac{y}{\text{dim}_y},$$

with a maximal inflow velocity C and a top/bottom boundary velocity set to zero. Again, we start with an initial grain of radius $2d$ in the center of a box Ω with dimensions $\text{dim}_x = 168d$ and $\text{dim}_y = 42d$. The simulation parameters are the same as above in the case of a rotating fluid.

The shape of the growing crystal is influenced by the fluid, which induces an anisotropy. This can be seen in Fig. 6, where the shape corresponding to a fluid velocity $C = 0.15$ is shown in a clipping of the whole domain Ω . The flow direction is from left to right. The particle density ψ is shown in the left image together with the velocity relative to the velocity of the translating crystal, i.e., $\mathbf{v}_{\text{crystal}} = (v_{\text{crystal}}, 0)^T$ with $v_{\text{crystal}} \approx 0.124$. The right image shows in the upper half, the absolute value of the velocity, with a constant value within the crystal, and in the lower half, the flow velocity relative to the initial velocity \mathbf{u}_0 . This shows an elongated vortex. In the case of no fluid coupling, the crystal grows isotropically to a circular shape, as in the example above.

Thus, also for Poiseuille flow, we see a coupling in both directions, the shape of the crystal is influenced by the flowing environment, and the fluid velocity is influenced by the crystal.

B. Sedimentation

In the following, we apply the NS-PFC model to a collection of individual particles to show the applicability as a model for particle dynamics. We therefore consider \mathcal{F}_{pfc} . For penalty term (27), we use the parameters $(n, \beta) = (3, 2000)$ in all of the following simulations. The Reynolds number and viscosity ratio are chosen as before, but the viscosity profile is now

given by

$$\phi := \psi_{(0)} \approx \frac{\psi}{\max_{\Omega}(\psi)}.$$

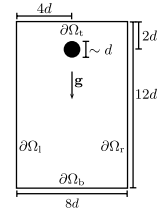
Thus, we have the lower fluid viscosity away from the particles and a high viscosity on the particles. In order to stabilize the shape of the particles, we increase the diffusional part, i.e., the Peclet number Pe , respective to the mobility function $M(\psi)$. We have chosen $M(\psi) \equiv 16$ in the following examples.

1. One spherical particle in a confinement

The objective of this study is to calculate the position and velocity of one spherical particle (circular disk) settling down in an enclosure due to a gravitational force \mathbf{g} . In order to include this force, we use a Bousinesq approximation and add the forcing term $\mathbf{F}_g := \phi(\psi)\mathbf{g}$ to Navier-Stokes equations in (28).

The box dimensions are chosen to be multiples of the particle size. All lengths are again normalized by the particle interaction distance $d = 4\pi/\sqrt{3}$, i.e., the lattice constant. We consider the following boundary conditions:

$$\begin{aligned} \psi &= 0 & \text{at } \partial\Omega_l \cup \partial\Omega_r \cup \partial\Omega_b, \\ \partial_n \psi &= 0 & \text{at } \partial\Omega_t, \\ \mathbf{u} &= 0 & \text{at } \partial\Omega_l \cup \partial\Omega_r \cup \partial\Omega_b, \\ \bar{\sigma} \cdot \mathbf{n}_{\Sigma} &= 0 & \text{at } \partial\Omega_t, \end{aligned}$$



with \mathbf{n}_{Σ} the outer normal to $\Sigma := \partial\Omega$.

Due to the symmetry of the system, we expect a symmetric trajectory, a straight line in the center of the box with the particle slowing down at the bottom. Fig. 7 shows the $y(t)$ component of the evolution curve $(x(t), y(t))$ compared with FPD simulations. We further show the comparison of the velocity profiles. For both criteria, we obtain an excellent agreement.

In the FPD setup, we have used the normalized density field $\psi_{(0)}(\mathbf{r})$ as a concentration field instead of tanh-profile (17) and for treatment of the wall-boundary we have introduced a

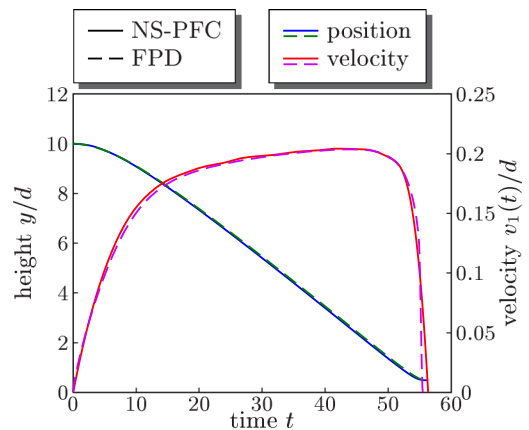


FIG. 7. Trajectory and velocity of one particle settling down in a box filled with a liquid with fluid viscosity $\bar{\eta}_f = 0.1$, particle viscosity $\bar{\eta}_p = 10$, and gravitational force $\mathbf{g} = (0, -1)$. Left: vertical position of the particle, starting from an initial height of $10d$. Right: effective velocity of the particle, i.e., $v_1(t)^2 = (\dot{x}(t)^2 + \dot{y}(t)^2)/d^2$.

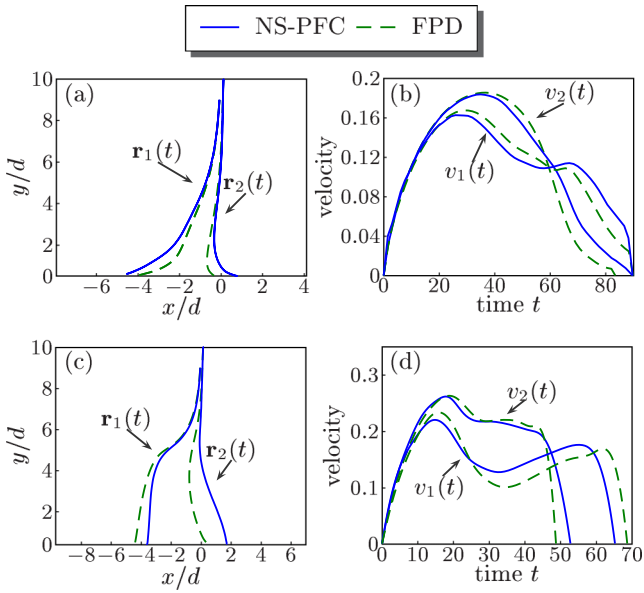


FIG. 8. Two particles settling down in an enclosure. Fluid viscosity is set to $\bar{\eta}_f = 1$ (a) and (b) and $\bar{\eta}_f = 0.1$ (c,d), particle viscosity to $\bar{\eta}_p = 100$ (a,b), and $\bar{\eta}_p = 10$ (c) and (d) and mobility of the NS-PFC-model to $M(\psi) \equiv 2$. Left: trajectories of the particles with coordinates $\mathbf{r}_i(t) = (x_i(t), y_i(t))$, $i = 1, 2$. Right: absolute velocities: $v_i(t)^2 = (x_i(t)^2 + y_i(t)^2)/d^2$, $i = 1, 2$.

repulsive potential

$$\mathcal{V}_B(k, p)(\mathbf{r}) := k(d^{-1} \text{dist}_{\Sigma}(\mathbf{r}))^p,$$

with $k = 1, p = 20$, and $\text{dist}_{\Sigma}(\mathbf{r})$ the distance of \mathbf{r} to the boundary Σ of the domain Ω .

Further care is needed in order to guarantee a symmetric solution. Within both approaches, we use a symmetric triangulation of the domain and symmetric quadrature rules. Otherwise, we get symmetry breaking in the trajectories, since the motion on a straight line is unstable with respect to small perturbations, as it is also pointed out in the work of Ref. 24.

2. Two interacting particles

For two particles sedimenting in a box, additional hydrodynamic interactions are expected to influence the motion of the particles. We expect to see the phenomena of trailing, drafting, kissing, and tumbling of the particles, as found in experimental studies⁴⁵ and as also observed in several numerical studies with various methods, e.g., Refs. 24, 46, and 47. Again, we compare it with FPD simulations where we have to apply direct particle-particle interaction potentials, defined

as $\mathcal{V}(\mathbf{r}) := k((\frac{r}{d})^{p_1} - 2(\frac{r}{d})^{p_2})$, with $(k, p_1, p_2) = (1, 12, 6)$ and a boundary interaction potential \mathcal{V}_B as above. Since we do not have a one-to-one mapping between these potentials and their representation in $\mathcal{F}_{\text{vpfc}}$ and since the PFC-model introduces additional diffusion due to a non-vanishing mobility function $M(\psi)$, equality of particle trajectories and particle velocities cannot be expected. However, the results qualitatively agree for different fluid viscosities, as can be seen in Fig. 8. To analyze the dependency of the trajectories on the considered interaction potential \mathcal{V} , FPD simulations with different potentials, i.e., different parameters in the Lennard-Jones type interaction, and purely repulsive interactions are performed and compared with each other. The obtained differences in the trajectories and the particle velocities are in the same order as the differences if compared with the NS-PFC simulations (results not shown).

The system considered here consists of two particles placed below each other with a small (symmetric) displacement relative to the middle vertical axis. The initial configuration is chosen as $\mathbf{r}_1 = (-0.1d, 9d)$ and $\mathbf{r}_2 = (0.1d, 10d)$, with boundary conditions as for the case of one particle. Compared to the one-particle case, the box size is chosen wider, i.e., a width of $18d$ instead of $8d$, to further reduce boundary effects.

The solution can also be compared qualitatively to the results in Refs. 24 and 48, where the authors have studied the sedimentation of two hard sphere particles in a narrow enclosure in a similar setup and they have found similar trailing and drafting phenomena. However, they are not as strong as in the FPD or in our simulations. The particles start in close contact and accelerate up to a critical time, when they start moving apart from each other. In the visualized scenarios in Fig. 8, the particle behind overtakes the other one and reaches the bottom first. Compared with FPD in our simulations, the particles move further away from each other and the velocity decreases in a similar way up to the contact with the lower boundary.

3. Many particles in an enclosure

With three particles already, the interaction and motion of the particles becomes chaotic, as pointed out in Ref. 49 and discussed in detail in the review.⁵⁰ Therefore, a direct comparison of trajectories is no longer meaningful. However, considering not only a few but also a larger number of particles in a bounded box under gravity cause new effects. Particles do not settle down homogeneously; their dynamics strongly depend on the distance to the walls. During the sedimentation

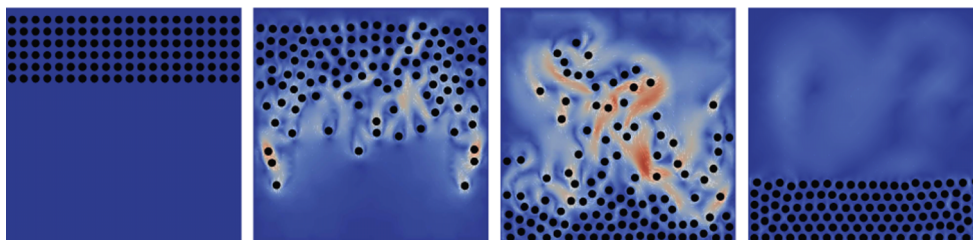


FIG. 9. Four snapshots of the sedimentation simulation for 120 particles in a square box. Color red corresponds to high absolute velocity and blue to low velocity. Left: initial configuration of particles. Second image: an instability of the particle front, starting from the boundaries. Third image: particles start to sediment at the bottom. Right: final compressed sediment of particles.

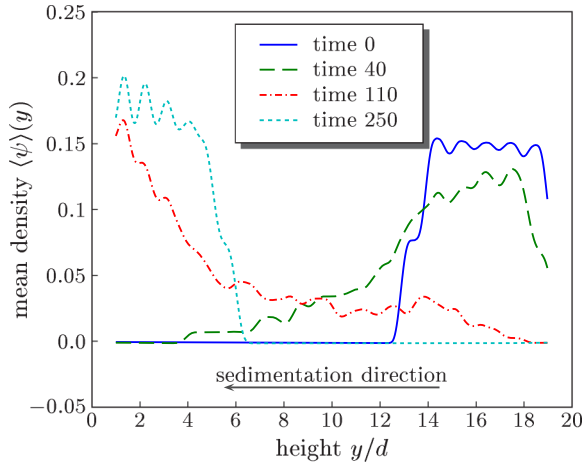


FIG. 10. Evolution of mean density of particles for four different time steps corresponding to the snapshots in Fig. 9. The final configuration of particles in a hexagonal lattice has a higher density than the initial configuration in a square lattice.

process, Rayleigh-Taylor-like instabilities and fingering occur and a compression of the particle lattice at the bottom of the box is seen. To demonstrate the possibility of our approach, to deal with moderate numbers of particles, we aim to observe these phenomena. We have studied a situation of 120 particles arranged in a square lattice in the upper part of a square domain. The initial distance of neighboring particles is set to the lattice constant d . The width of the box is chosen so that 20 particles fit perfectly in one horizontal line, i.e., we have $\dim_x = \dim_y = 20d$. Boundary conditions are chosen similar to the cases before. For a gravitational force $\mathbf{g} = (0, -2)^T$ we have simulated the sedimentation process in a fluid with a viscosity ratio $\bar{\eta}_p/\bar{\eta}_f = 100$, as above. The particles close to the side walls start settling down first and due to their motion, an upwards fluid flow in the center of the domain is induced. A visualization of the sedimentation process is shown in Fig. 9. We have drawn black circular disks to indicate the particle positions. Four snapshots are shown, the initial and final configuration and two intermediate states, i.e., the beginning of the development of the instability and a snapshot with partially sedimented particles.

In Fig. 10, the mean particle concentration $\langle \psi \rangle(y)$ is shown, which is obtained by averaging over stripes of width d along the particle layers,

$$\langle \psi \rangle(y) := \int_{x=x_{\min}}^{x_{\max}} \int_{y'=y-0.5d}^{y+0.5d} \psi(x, y') dy' dx.$$

The high-concentration region moves from top to bottom over time and the mean particle density is higher at the bottom of the box than for the initial configuration.

IV. CONCLUSION

A fully continuous model is developed to simulate colloidal particles in a fluid, interacting via direct particle-particle interaction and via the induced flow fields. The method is based on ideas of dynamic density functional theory and fully resolved direct numerical simulations. The derived NS-PFC

system operates on diffusive time scales and provides a qualitative approach down to the particle size.

We have demonstrated the quality of the method in various examples; first, in crystallization processes analyzing the influence of a macroscopic flow field and second, for three common test cases, namely, the sedimentation of one, two, and many particles. For one and two particles, we have quantitatively compared the trajectories and velocities obtained by our simulation to simulations with the FPD method and have found good agreement. For the case of many particles, we see the expected instabilities and compression at the bottom. For more quantitative comparisons, the calculation of a hydrodynamic radius would be desirable, as it is done by Refs. 3 and 12. However, this requires computations in 3D for the comparison with Stokes drag and drag torque and has thus to be considered in future work. As a preliminary step, we have computed the effective radius of the vacancy NS-PFC model by comparison with the FPD method, using concentration profile (17), for which a radius is given. We have computed the particle velocities obtained by both methods for one particle dragged through a periodic channel. Comparing the result for various radii for the FPD method, we find an effective radius for the NS-PFC model of approximately $0.35d$.

However, in comparison with the other methods mentioned in the Introduction, we do not see the advantages of our approach in a more detailed description of the underlying physics on a single particle scale, but in the emergent phenomena on larger scales. Here, the formulation as a fully continuous model has several numerical advantages: we expect stable numerical behavior. For the classical PFC equation time step, independent stability can be proven for the discrete scheme.^{51–53} Coupling this to the Navier-Stokes equation, as considered, e.g., in Ref. 54, allows for larger time steps as in the explicit coupling schemes of hybrid methods. As the NS-PFC model only contains local terms, the algorithms are expected to scale independently of the number of particles. Numerical details of an efficient parallel scheme are described in Ref. 53 for the classical PFC equation and can be extended towards the coupling with Navier-Stokes.

ACKNOWLEDGMENTS

This work has been funded through Grant Nos. DFG Vo899/11 and FP7 IRSES 247504. We further acknowledge the provided computing resources at ZIH at TU Dresden and JSC at FZ Jülich.

APPENDIX A: DIMENSIONLESS FORM

The density ϱ is driven by the variational derivative of the Helmholtz free energy \mathcal{F}_H . This functional can be decomposed into two contributions $\mathcal{F}_H = \mathcal{F}_{\text{id}} + \mathcal{F}_{\text{exc}}$, where the ideal gas part \mathcal{F}_{id} is known and the excess free part unknown for general systems,

$$\mathcal{F}_H[\varrho] = k_B T \int \varrho [\ln(\Lambda^d \varrho) - 1] d\mathbf{r} + \mathcal{F}_{\text{exc}}[\varrho],$$

with k_B Boltzmann's constant, T the temperature, Λ the thermal de-Broglie wave-length, and d the space dimension.

Inserting a parametrization $\varrho = \varrho(\varphi) = \bar{\varrho}(1 + \varphi)$ with the density deviation φ and reference density $\bar{\varrho}$ into the energy and expanding the ideal gas part of the energy around $\bar{\varrho}$ leads to a polynomial form of \mathcal{F}_{id} . Using a Ramakrishnan-Yussouff approximation⁵⁵ of the excess free part results in an expression of the two-point correlation function $c^{(2)}(\mathbf{r}, \mathbf{r}', \varrho)$,

$$\mathcal{F}_{\text{exc}} = C + \iint (\varrho(\mathbf{r}) - \varrho_L) c^{(2)}(\mathbf{r}, \mathbf{r}', \varrho_L) (\varrho(\mathbf{r}') - \varrho_L) d\mathbf{r} d\mathbf{r}',$$

with ϱ_L a reference liquid density. This corresponds to a convolution of $(\varrho - \varrho_L)$ with $c^{(2)}$ and can thus be transformed into a product in Fourier space. Expanding $c^{(2)}$ around the wave-number zero and transforming back lead to a gradient expansion of \mathcal{F}_{exc} that can be written in the variable φ ,

$$\begin{aligned} \frac{1}{k_B T \bar{\varrho}} (\mathcal{F}_{\text{H}}[\varrho(\varphi)] - \bar{\mathcal{F}}_{\text{H}}) &\approx \int \frac{1}{2} \varphi^2 - \frac{1}{6} \varphi^3 + \frac{1}{12} \varphi^4 d\mathbf{r} \\ &- \int \frac{1}{2} \varphi (C_0 - C_2 \Delta + C_4 \Delta^2) \varphi d\mathbf{r} \\ &+ \int D_0 + D_1 \varphi d\mathbf{r}, \end{aligned}$$

with C_0, C_2, C_4, D_0, D_1 expansion coefficients. For a detailed derivation, see, e.g., Refs. 21–23. Since we take the gradient of the variational derivative in the dynamical equations, all constant and linear terms can be neglected in the energy without changing the dynamics.

Fixing the lattice spacing L , the dimensionless bulk modulus of the crystal B and introducing parameters r and ψ_0 , with

$$\begin{aligned} L^2 &:= \frac{2|C_4|}{C_2}, & B &:= \frac{C_2^2}{4|C_4|} = \frac{\psi_0^2}{3}, \\ \text{sign}(C_4) &= -1, & r &:= \psi_0^{-2} \left(\frac{9}{4} - 3C_0 \right) - 1, \end{aligned}$$

scaling the length by L , i.e., $\hat{\mathbf{r}} = \mathbf{r}/L$, and introducing the derivatives $\hat{\nabla} := \partial_{\hat{\mathbf{r}}}$, $\hat{\Delta} = \hat{\nabla} \cdot \hat{\nabla}$ and a new variable $\psi = \psi(\hat{\mathbf{r}})$ as

$$\varrho(\mathbf{r}) = \bar{\varrho}(\psi_0 \cdot (\psi \circ \hat{\mathbf{r}})(\mathbf{r}) + 1.5),$$

with $(\psi \circ \hat{\mathbf{r}})(\mathbf{r}) = \psi(\hat{\mathbf{r}}(\mathbf{r}))$, where \circ acts as a function composition operator, result in the classical PFC energy

$$\begin{aligned} \frac{3}{k_B T \bar{\varrho} \psi_0^4} (\mathcal{F}_{\text{H}}[\varrho(\psi)] - \bar{\mathcal{F}}_{\text{H}}) &\approx L^d \int \frac{1}{2} (1+r) \psi^2 + \frac{1}{4} \psi^4 \\ &+ \psi \hat{\Delta} \psi + \frac{1}{2} \psi \hat{\Delta}^2 \psi d\hat{\mathbf{r}} \\ &=: L^d \mathcal{F}_{\text{sh}}[\psi]. \end{aligned}$$

We consider the variational derivative of \mathcal{F}_{H} and relate it to the variational derivative of \mathcal{F}_{sh} ,

$$\begin{aligned} \frac{\delta \mathcal{F}_{\text{H}}[\varrho]}{\delta \varrho} &= \frac{1}{L^d} \left(\frac{\delta \mathcal{F}_{\text{H}}[\varrho \circ \mathbf{r}]}{\delta(\varrho \circ \mathbf{r})} \circ \hat{\mathbf{r}} \right) \\ &\approx \frac{1}{L^d} \left(\frac{\delta \left(\frac{1}{3} k_B T \bar{\varrho} \psi_0^4 L^d \mathcal{F}_{\text{sh}}[\psi] + \bar{\mathcal{F}}_{\text{H}} \right)}{\delta(\varrho \circ \mathbf{r})} \circ \hat{\mathbf{r}} \right) \\ &= \frac{1}{3} k_B T \bar{\varrho} \psi_0^4 \left(\frac{\delta \mathcal{F}_{\text{sh}}[\psi]}{\delta \psi} \frac{\delta \psi}{\delta(\varrho \circ \mathbf{r})} \circ \hat{\mathbf{r}} \right) \\ &= \frac{1}{3} k_B T \psi_0^3 \left(\frac{\delta \mathcal{F}_{\text{sh}}[\psi]}{\delta \psi} \circ \hat{\mathbf{r}} \right). \end{aligned}$$

Inserting the parametrization of ϱ into dynamical equations (1) and (2), fixing $\psi_0 = 1$ for simplicity and using the length

scaling $\hat{\mathbf{r}}$ give

$$\begin{aligned} (1.5 + \psi)(\partial_t \mathbf{v} + \frac{1}{L} (\mathbf{v} \cdot \hat{\nabla}) \mathbf{v} + \gamma \mathbf{v}) &= \frac{k_B T}{3mL} \hat{\nabla} \frac{\delta \mathcal{F}_{\text{sh}}[\psi]}{\delta \psi} \\ &+ \frac{\eta}{m \bar{\varrho} L^2} \hat{\Delta} \mathbf{v}, \\ \partial_t \psi &= -\frac{1}{L} \hat{\nabla} \cdot ((1.5 + \psi) \mathbf{v}). \end{aligned}$$

Introducing the dimensionless variables $\hat{t} := tV_0/L$ and $\hat{\mathbf{v}} := \mathbf{v}/V_0$ finally gives the dimensionless dynamical equations

$$\begin{aligned} (1.5 + \psi)(\partial_{\hat{t}} \hat{\mathbf{v}} + (\hat{\mathbf{v}} \cdot \hat{\nabla}) \hat{\mathbf{v}} + \frac{\gamma L}{V_0} \hat{\mathbf{v}}) &= \frac{k_B T}{3mV_0^2} \hat{\nabla} \frac{\delta \mathcal{F}_{\text{sh}}}{\delta \psi} \\ &+ \frac{\eta}{m \bar{\varrho} L V_0} \hat{\Delta} \hat{\mathbf{v}}, \\ \partial_{\hat{t}} \psi &= -\hat{\nabla} \cdot ((1.5 + \psi) \hat{\mathbf{v}}). \end{aligned}$$

By defining the dimensionless numbers

$$Pe = \frac{3mV_0^2}{k_B T}, \quad Re = \frac{m \bar{\varrho} L V_0}{\eta} \quad \text{and} \quad \Gamma = \frac{\gamma L}{V_0}$$

as above, we find Eqs. (4)–(5), where we have neglected the hat symbol on the derivatives for readability.

APPENDIX B: ENERGY DISSIPATION

To demonstrate thermodynamic consistency of the model, we assume that the total energy of the system is composed of the Helmholtz free-energy \mathcal{F}_{H} , respective to an appropriate approximation of this functional and the kinetic energy

$$\mathcal{F}_{\text{kin}} = \frac{\rho_f}{2} \int \|\mathbf{u}\|^2 d\mathbf{r}$$

of the surrounding fluid. To be consistent with dynamical equations (28), we focus on the dimensionless energies by introducing length and time scales as above and by defining dimensionless variables denoted by a hat symbol. Additionally, we normalize the energies

$$\hat{\mathbf{r}} = \mathbf{r}/L, \quad \hat{t} = tV_0/L, \quad \hat{\mathbf{u}} = \mathbf{u}/V_0, \quad \hat{\mathcal{F}}_* = \mathcal{F}_*/(V_0 L^2 \bar{\eta}_f).$$

This gives us the dimensionless kinetic energy

$$\hat{\mathcal{F}}_{\text{kin}} = \frac{Re_f}{2} \int \|\hat{\mathbf{u}}\|^2 d\hat{\mathbf{r}}$$

and by considering the correct scaling of the Swift-Hohenberg energy $\mathcal{F}_{\text{H}} \approx k_B T \bar{\varrho} \frac{L^3}{3} \mathcal{F}_{\text{sh}}$ (see Appendix A), we find

$$\hat{\mathcal{F}}_{\text{H}} = \frac{1}{Sc} \int \frac{1}{4} \psi^4 + \frac{1}{2} \psi (r + (q_0^2 + \Delta)^2) \psi d\hat{\mathbf{r}},$$

with the Schmidt number Sc given by

$$Sc = \frac{Pe}{Re_f} \bar{\varrho}, \quad \text{with} \quad \bar{\varrho} := \frac{\rho_f}{m \bar{\varrho}}.$$

The total dimensionless energy, to be considered, now reads

$$\hat{\mathcal{F}}_{\text{tot}} = \hat{\mathcal{F}}_{\text{kin}} + \hat{\mathcal{F}}_{\text{H}}.$$

In the following, we consider only nondimensional variables and for readability drop the hat symbols.

We assume that the evolution equations for momentum and mass conservation read

$$\begin{aligned}\partial_t \mathbf{u} + (\mathbf{u} \cdot \nabla) \mathbf{u} &= \nabla \cdot \tilde{\boldsymbol{\sigma}} + \mathbf{F}, \\ \nabla \cdot \mathbf{u} &= 0, \\ \partial_t \psi + \mathbf{u} \cdot \nabla \psi &= -\nabla \cdot \mathbf{j},\end{aligned}\quad (\text{B1})$$

where the volume force \mathbf{F} and the flux \mathbf{j} need to be determined to justify thermodynamic consistency. Let Ω be a fixed domain with Lipschitz-boundary Σ . The time-evolution of the energy \mathcal{F}_{tot} can be split into

$$\begin{aligned}\dot{\mathcal{F}}_{\text{kin}} &= Re_f \int_{\Omega} \mathbf{u} \cdot \partial_t \mathbf{u} \, \text{d}\mathbf{r} \\ &= Re_f \int_{\Omega} \mathbf{u} \cdot (-\mathbf{u} \cdot \nabla) \mathbf{u} + \nabla \cdot \tilde{\boldsymbol{\sigma}} + \mathbf{F} \, \text{d}\mathbf{r}, \\ \dot{\mathcal{F}}_{\text{H}} &= \frac{1}{Sc} \int_{\Omega} \frac{\delta \mathcal{F}_{\text{sh}}[\psi]}{\delta \psi} \partial_t \psi \, \text{d}\mathbf{r}.\end{aligned}\quad (\text{B2})$$

Using incompressibility and integration by parts and the relations

$$\begin{aligned}\frac{1}{2} \nabla (\|\mathbf{u}\|^2) &= (\mathbf{u} \cdot \nabla) \mathbf{u} - (\nabla \times \mathbf{u}) \times \mathbf{u}, \\ (f \nabla \mathbf{u}, \mathbf{D}(\mathbf{u}))_{\Omega} &= (f \mathbf{D}(\mathbf{u}), \mathbf{D}(\mathbf{u}))_{\Omega},\end{aligned}$$

for a scalar field $f = f(\mathbf{r})$ and the inner product $(\mathbf{A}, \mathbf{B})_{\Omega} = \int_{\Omega} \mathbf{A} : \mathbf{B} \, \text{d}\mathbf{r}$, we get

$$\begin{aligned}\int_{\Omega} \mathbf{u} \cdot (\mathbf{u} \cdot \nabla) \mathbf{u} &= \int_{\Omega} \frac{1}{2} \mathbf{u} \cdot \nabla (\|\mathbf{u}\|^2) + \mathbf{u} \cdot [(\nabla \times \mathbf{u}) \times \mathbf{u}] \, \text{d}\mathbf{r} \\ &= \frac{1}{2} \int_{\Sigma} (\mathbf{u} \cdot \mathbf{n}_{\Sigma}) \|\mathbf{u}\|^2 \, \text{d}\Sigma \\ &= 0 \text{ for } \begin{cases} \mathbf{u} \cdot \mathbf{n}_{\Sigma} = 0, & \text{(no-penetration),} \\ \mathbf{u} = 0, & \text{(no-slip),} \end{cases} \\ \int_{\Omega} \mathbf{u} \cdot \nabla \cdot \tilde{\boldsymbol{\sigma}} \, \text{d}\mathbf{r} &= \underbrace{\int_{\Omega} -\nabla \mathbf{u} : \tilde{\boldsymbol{\sigma}} \, \text{d}\mathbf{r}}_{\leq 0} + \underbrace{\int_{\Sigma} \mathbf{u} \cdot \tilde{\boldsymbol{\sigma}} \cdot \mathbf{n}_{\Sigma} \, \text{d}\Sigma}_{(*)} \\ (*) = 0 \text{ for } &\begin{cases} \tilde{\boldsymbol{\sigma}} \cdot \mathbf{n}_{\Sigma} = 0, & \text{(no-flux),} \\ \mathbf{u} = 0, & \text{(no-slip).} \end{cases}\end{aligned}$$

Thus, we get for the kinetic part of the energy, in case of no-slip boundary conditions, the estimate

$$\dot{\mathcal{F}}_{\text{kin}} \leq Re_f \int_{\Omega} \mathbf{u} \cdot \mathbf{F} \, \text{d}\mathbf{r}.$$

The derivative of the PFC-part of the energy evolution reads

$$\dot{\mathcal{F}}_{\text{H}} = \frac{1}{Sc} \int_{\Omega} \mathbf{j} \nabla \frac{\delta \mathcal{F}_{\text{sh}}[\psi]}{\delta \psi} - \mathbf{u} \cdot \frac{\delta \mathcal{F}_{\text{sh}}[\psi]}{\delta \psi} \nabla \psi \, \text{d}\mathbf{r}.$$

By choosing the flux \mathbf{j} proportional to $-\nabla \delta \mathcal{F}_{\text{sh}}[\psi] / \delta \psi$, e.g.,

$$\mathbf{j} = -M(\psi) \nabla \frac{\delta \mathcal{F}_{\text{sh}}[\psi]}{\delta \psi},$$

with $M(\psi)$ any positive definite function, we find for the total energy evolution

$$\dot{\mathcal{F}}_{\text{tot}} \leq \int_{\Omega} \mathbf{u} \cdot \left[Re_f \mathbf{F} - \frac{1}{Sc} \frac{\delta \mathcal{F}_{\text{sh}}[\psi]}{\delta \psi} \nabla \psi \right] \, \text{d}\mathbf{r}$$

and can choose \mathbf{F} so that this integral vanishes, i.e.,

$$\mathbf{F} = \frac{1}{Re_f Sc} \frac{\delta \mathcal{F}_{\text{sh}}[\psi]}{\delta \psi} \nabla \psi = \frac{\bar{\varrho}}{Pe} \frac{\delta \mathcal{F}_{\text{sh}}[\psi]}{\delta \psi} \nabla \psi.$$

Using incompressibility again, we get the relation to the force and flux terms derived before. For no-slip boundary conditions, we have

$$\int_{\Omega} -\frac{1}{Sc} \mathbf{u} \cdot \frac{\delta \mathcal{F}_{\text{sh}}[\psi]}{\delta \psi} \nabla \psi \, \text{d}\mathbf{r} = \int_{\Omega} \frac{1}{Sc} \mathbf{u} \cdot \psi \nabla \frac{\delta \mathcal{F}_{\text{sh}}[\psi]}{\delta \psi} \, \text{d}\mathbf{r}$$

and thus, the force

$$\mathbf{F} = -\frac{\bar{\varrho}}{Pe} \psi \nabla \frac{\delta \mathcal{F}_{\text{sh}}[\psi]}{\delta \psi} \quad (\text{B3})$$

and with $M_1 = \bar{\varrho}/Pe$, the above set of Eq. (28). Our derived continuum model thus fulfills thermodynamic consistency.

- ¹A. Furukawa and H. Tanaka, *Phys. Rev. Lett.* **104**, 245702 (2010).
- ²Y. Matsuoka, T. Fukasawa, K. Higashitani, and R. Yamamoto, *Phys. Rev. E* **86**, 051403 (2012).
- ³J. Padding and A. Louis, *Phys. Rev. E* **74**, 031402 (2006).
- ⁴J. F. Brady and G. Bossis, *Annu. Rev. Fluid Mech.* **20**, 111 (1988).
- ⁵P. J. Hoogerbrugge and J. M. V. A. Koelman, *Europhys. Lett.* **19**, 155 (1992).
- ⁶P. Español and M. Revenga, *Phys. Rev. E* **67**, 026705 (2003).
- ⁷S. Litvinov, M. Ellero, X. Hu, and N. A. Adams, *Phys. Rev. E* **77**, 066703 (2008).
- ⁸C. S. Peskin, *Acta Numerica* **11**, 479 (2002).
- ⁹R. Glowinski, T.-W. Pan, T. I. Hesla, and D. D. Joseph, *Int. J. Multiphase Flow* **25**, 755 (1999).
- ¹⁰J. Onishi, A. Kawasaki, Y. Chen, and H. Ohashi, *Comput. Math. Appl.* **55**, 1541 (2008).
- ¹¹A. S. Joshi and Y. Sun, *Phys. Rev. E* **79**, 066703 (2009).
- ¹²S. T. T. Ollila, C. J. Smith, T. Ala-Nissila, and C. Denniston, *Multiscale Model. Simul.* **11**, 213 (2013).
- ¹³M. Fujita and Y. Yamaguchi, *Curr. Opin. Colloid Interface Sci.* **15**, 8 (2010).
- ¹⁴U. M. B. Marconi and P. Tarazona, *J. Phys.: Condens. Matter* **12**, A413 (2000).
- ¹⁵A. J. Archer, *J. chem. phys.* **130**, 014509 (2009).
- ¹⁶M. Rauscher, A. Dominguez, M. Kruger, and F. Penna, *J. Chem. Phys.* **127**, 244906 (2007).
- ¹⁷B. D. Goddard, A. Nold, N. Savva, P. Yatsyshin, and S. Kalliadasis, *J. Phys.: Condens. Matter* **25**, 035101 (2013).
- ¹⁸G. I. Tóth, L. Gránásy, and G. Tegze, *J. Phys.: Condens. Matter* **26**, 055001 (2014).
- ¹⁹J. Swift and P. C. Hohenberg, *Phys. Rev. A* **15**, 319 (1977).
- ²⁰K. Elder, M. Katakowski, M. Haataja, and M. Grant, *Phys. Rev. Lett.* **88**, 245701 (2002).
- ²¹S. van Teeffelen, R. Backofen, A. Voigt, and H. Löwen, *Phys. Rev. E* **79**, 051404 (2009).
- ²²A. Jaatinen, "Modeling materials with phase field crystal models," Ph.D. thesis (Aalto University School of Science and Technology, 2010).
- ²³S. Praetorius and A. Voigt, *Macromol. Theory Simul.* **20**, 541 (2011).
- ²⁴R. Glowinski, T. W. Pan, T. I. Hesla, D. D. Joseph, and J. Périaux, *J. Comput. Phys.* **169**, 363 (2001).
- ²⁵M. Uhlmann, *J. Comput. Phys.* **209**, 448 (2005).
- ²⁶S. V. Apte, M. Martin, and N. A. Patankar, *J. Comput. Phys.* **228**, 2712 (2009).
- ²⁷T. Kempe and J. Fröhlich, *J. Comput. Phys.* **231**, 3663 (2012).
- ²⁸H. Tanaka and T. Araki, *Phys. Rev. Lett.* **85**, 1338 (2000).
- ²⁹E. Siggia, B. Halperin, and P. Hohenberg, *Phys. Rev. B* **13**, 2110 (1976).
- ³⁰P. Hohenberg and B. Halperin, *Rev. Mod. Phys.* **49**, 435 (1977).
- ³¹Y. Nakayama and R. Yamamoto, *Phys. Rev. B* **71**, 036707 (2005).
- ³²A. M. Menzel and H. Löwen, *Phys. Rev. Lett.* **110**, 055702 (2013).
- ³³P. Y. Chan, N. Goldenfeld, and J. Dantzig, *Phys. Rev. B* **79**, 035701 (2009).
- ³⁴J. Berry and M. Grant, *Phys. Rev. Lett.* **106**, 175702 (2011).
- ³⁵X. Li, J. Lowengrub, A. Rätz, and A. Voigt, *Commun. math. sci.* **7**, 81 (2009).
- ³⁶S. Franz, R. Gärtner, H. Roos, and A. Voigt, *Comput. Methods Appl. Math.* **12**, 121 (2012).
- ³⁷K. R. Elder and M. Grant, *Phys. Rev. E* **70**, 051605 (2004).
- ³⁸M. Rauscher, *J. Phys.: Condens. Matter* **22**, 364109 (2010).
- ³⁹U. Thiele, A. J. Archer, M. J. Robbins, H. Gomez, and E. Knobloch, *Phys. Rev. E* **87**, 042915 (2013).
- ⁴⁰M. J. Robbins, A. J. Archer, U. Thiele, and E. Knobloch, *Phys. Rev. E* **85**, 061408 (2012).

- ⁴¹D. Jacqmin, *J. Comput. Phys.* **155**, 32 (1999).
- ⁴²O. Axelsson and M. Neytcheva, "Operator splittings for solving nonlinear, coupled multiphysics problems with an application to the numerical solution of an interface problem," Tech. Rep. No. 2011-009 (Department of Information Technology, Uppsala University, 2011).
- ⁴³S. Vey and A. Voigt, *Comput. Visualization Sci.* **10**, 57 (2007).
- ⁴⁴T. Witkowski, S. Ling, and A. Voigt, *Adv. Comput. Math.* **2015**, 1 (2015).
- ⁴⁵A. F. Fortes, D. D. Joseph, and T. S. Lundgren, *J. Fluid Mech.* **177**, 467 (2006).
- ⁴⁶H. H. Hu, D. D. Joseph, and M. J. Crochet, *Theor. Comput. Fluid Dyn.* **3**, 285 (1992).
- ⁴⁷J. B. Ritz and J. P. Caltagirone, *Int. J. Numer. Methods Fluids* **30**, 1067 (1999).
- ⁴⁸S. Lin, Y. Chin, J. Hu, and Y. Chen, *Int. J. Numer. Methods Fluids* **67**, 1771 (2011).
- ⁴⁹I. M. Jánosi, T. Tél, D. E. Wolf, and J. A. C. Gallas, *Phys. Rev. E* **56**, 2858 (1997).
- ⁵⁰S. Ramaswamy, *Adv. Phys.* **50**, 297 (2001).
- ⁵¹R. Backofen, A. Rätz, and A. Voigt, *Philos. Mag. Lett.* **87**, 813 (2007).
- ⁵²S. M. Wise, C. Wang, and J. S. Lowengrub, *SIAM J. Numer. Anal.* **47**, 2269 (2009).
- ⁵³S. Praetorius and A. Voigt, "Development and analysis of a block-preconditioner for the phase-field crystal equation," *SIAM J. Sci. Comput.* e-print [arXiv: 1501.06852](https://arxiv.org/abs/1501.06852) (to be published).
- ⁵⁴S. Aland, *J. Comput. Phys.* **262**, 58 (2014).
- ⁵⁵T. Ramakrishnan and M. Yussouff, *Phys. Rev. B* **19**, 2775 (1979).